Experimental Study on Floor Damage and Slurry Material Ratio Optimization in Deep and High Confined Water Mining

Wenmiao Wang [1,2], Yong Yuan [1,2,*], Xiaokang Liang [1,2,3,*], Zhenghan Qin [1,2], Zhongshun Chen [1,2], Ke Ding [2,4], Yongqi Xia [1,2] and Chenlong Yan [1,2]

1. Key Laboratory of Deep Coal Resource, Ministry of Education of China, China University of Mining & Technology, Xuzhou 221116, China
2. School of Mines, China University of Mining & Technology, Xuzhou 221116, China
3. Shaanxi Energy Fengjiata Mining Operation Co., Ltd., Yulin 719400, China
4. State Key Laboratory for Geomechanics and Deep Underground Engineering, China University of Mining and Technology, Xuzhou 221116, China
* Correspondence: cumt-yuanyong@cumt.edu.cn (Y.Y.); 15339096934@163.com (X.L.)

Abstract: Deep mining has started in the Huaibei mining area, and the serious threat of high confined water on the floor to the coal seam is gradually increasing. Based on the deep confined water mining project at working face II633 of the Hengyuan coal mine, this paper theoretically analyzes the damage depth of the floor and the risk of water inrush from the floor. The best proportion of grouting materials was quantitatively optimized by indoor experiments, and an industrial field test was conducted to judge the grouting effect. The results show that the failure depth of the bottom plate calculated by theoretical analysis is 31.73 m; a single factor test and a response surface optimization design method determined the best value of each index: water cement ratio 0.8, bentonite 2%, water reducer 0.6%, sodium silicate 2%. The damage depth of the bottom plate after grouting is 18.83~20 m, according to the field monitoring by the strain method. The optimized slurry significantly reduces the damage depth of the floor, ensures the safe and efficient mining of the coal seam above the high–pressure water, and has a high reference value for the safe mining of the coal seam under similar geological conditions.

Keywords: mining above confined water; response surface design; optimization of slurry ratio; field measurement

1. Introduction

As time progresses, fossil energy, such as coal, is gradually being replaced by new clean energy, but at present, the role of coal as China's "energy ballast" is still irreplaceable [1–3]. At present, China's shallow coal resources are increasingly scarce, and the mining level of mines is gradually extending to new depths at the speed of 10–15 m/a [4]. The mining depths of Huaibei, Shandong, and other mining areas in China have reached more than 1000 m, and the coal resources below 1000 km account for 53% of the total proven coal resources [5,6]. During deep mining, the working face is greatly affected by "three highs and one disturbance". Especially in the North China mining area, confined water is abundant. Under the coupling effect of mining stress and confined water pressure, the floor aquiclude of the coal seam floor is "exhausted", which is very prone to floor water inrush accidents, seriously restricting the safe production and smooth replacement of the mining operation [7–9]. According to the data, more than 50% of coal mines in China are threatened by confined floor water. Therefore, how to safely mine the coal resources threatened by high confined water has become a technical problem for the green transformation of relevant mines and the realization of the "double carbon" goal. In the past, most mines used mining methods such as short–wall, room and pillar, or strip–mining methods, which reduce the risk of water inrush from the floor. However, due to the large amount of coal left by such

methods, the coal loss rate is large, and more than 90% of underground coal mines in China mostly use long wall working faces. At present, the main methods to control the threat of water inrush from the floor are grouting reinforcement, drainage, and pressure reduction. Considering that dewatering and depressurization will cause secondary disasters such as damage to the groundwater environment, the method of floor grouting reinforcement is mostly used on site to reduce the depth of the floor damage and thus reduce the risk of floor water inrush [10,11]. Therefore, it is urgent to conduct in–depth research on the mechanisms of water inrush from the floor and the prevention and control of water inrush by grouting reinforcement of the floor.

In recent years, domestic and foreign experts and scholars have used theoretical analysis, numerical simulation, and other research methods to evaluate and predict the risk of water inrush from the mechanism of floor water inrush and the development of floor fissures and have achieved remarkable results [12–16]. For example, Yu, Xu et al. [17,18] used BP neural network, linear regression, and other methods to predict the depth of floor damage and predicted and analyzed the possibility of floor water inrush. In order to further clarify the stress characteristics of the floor, Ma et al. [19] used the elastic theory calculation, regarded the floor as a semi–infinite body model, and studied the evolution law of mining stress in the floor under the action of confined water. Song and Liang [20,21], based on the theory of elastic mechanics, calculated the damage form and water inrush danger area in the three–dimensional space of the floor and concluded that the water inrush danger area of the floor coincided with the maximum damage depth of the floor. The above theoretical research has a certain role in promoting and developing the damage mechanism of the floor, but it fails to consider the impact of complex factors such as actual geology and floor mining damage. Numerical simulation provides new research ideas and methods for solving the characteristics of floor failure and preventing floor water inrush. Yang Chen et al. [22] studied the depth of floor failure under different surrounding rock conditions and mining heights on confined water on the basis of three–dimensional finite difference simulation software FLAC3D, and combined with periodic pressure step, revealed the mechanism of periodic pressure on the peak strain of floor. Li and Zhu et al. [23,24] and others used fluid–solid coupling simulation software to reveal the water resistance performance of different rock combinations in the floor under the influence of confined water and mining coupling. In addition, some scholars have used ground penetrating radar, borehole peeping, microseismical monitoring, transient electromagnetic, and optical fiber measurement methods to observe and analyze the depth of damage to the floor and the dynamic evolution of cracks [25–28]. These methods can effectively and intuitively predict and evaluate the macro deformation of the floor and the risk of water inrush but do not take relevant measures in advance to analyze the shape of the floor crack development is inhibited.

Some scholars have also undertaken systematic and in–depth research on the safe mining of deep high–confined water coal seams from the aspects of floor grouting reinforcement and the slurry ratio [29–31] and provided theoretical guidance for floor reinforcement. Xu et al. [32], based on the measured floor resistivity, studied the initiation, development, and water–filling dynamic evolution process of floor water inrush channels in the mining process, and, based on this, predicted the floor water inrush. Cao et al. [33] analyzed the possible area of water inrush from the floor of the working face by using three–pole detection technology of the direct current method and adopted reasonable grouting parameters to reinforce the abnormal area by grouting. Some researchers have used drainage and pressure reduction, curtain closure, and other methods to prevent and control water inrush from the floor, but these methods are costly and will cause secondary disasters such as surface subsidence and groundwater level decline.

Therefore, in order to ensure the safe mining of coal seams above confined water, the grouting effect must be improved, and the grouting cost must be reduced. This paper used the mining activity above the confined water of the Hengyuan coal mine as the research background and adopted theoretical analysis to deduce the stress characteristics of the floor

under the action of the confined water of the floor. Combined with the empirical formula, the depth of the floor damage was determined to realize the risk analysis of water inrush from the floor. In addition, through indoor experiments, the grouting slurry ratio was optimized. Taking the slurry water separating proportion, slurry viscosity, setting time, and the compressive strength of the grouting stone body as evaluation indicators, the optimal slurry ratio was determined using a single factor test, weight analysis, and other methods, and this ratio was applied to the Hengyuan coal mine. Finally, the floor strain method was adopted, and the strain sensor penetrated different floor depths. The deformation and failure law of the floor in the process of coal mining was continuously monitored so as to evaluate and analyze the reinforcement effect on the floor. The research results of this paper can provide theoretical support and technical guidance for water inrush risk prediction and water disaster prevention for the mining floors above confined water in North China.

2. Geology and Hydrology of the Study Area

2.1. Geology of Study Area Overview

The Hengyuan coal mine is located in the Suixiao mining area of the Huaibei coalfield, which is located 10 km west of Suixi County, Huaibei City, Anhui Province. The geographical location of the mine is shown in Figure 1. The coal–bearing strata of the mine are the Shanxi Formation (P_{1S}) and the Lower Shihezi Formation (P_{1Xs}) of the lower Permian system. The coal–bearing strata are 343.20 m, including eight coal seams (groups) and 2~17 coal seams. The total thickness of the #3 coal seam is 5.52 m. The average total thickness of the minable or locally minable coal seams is 4.82 m, accounting for 87.3% of the total thickness of the coal seams. Among them, the #4 and #6 coal seams are the main minable coal seams, with an average total thickness of 4.48 m, accounting for 81.2% of the total thickness of the minable coal seams.
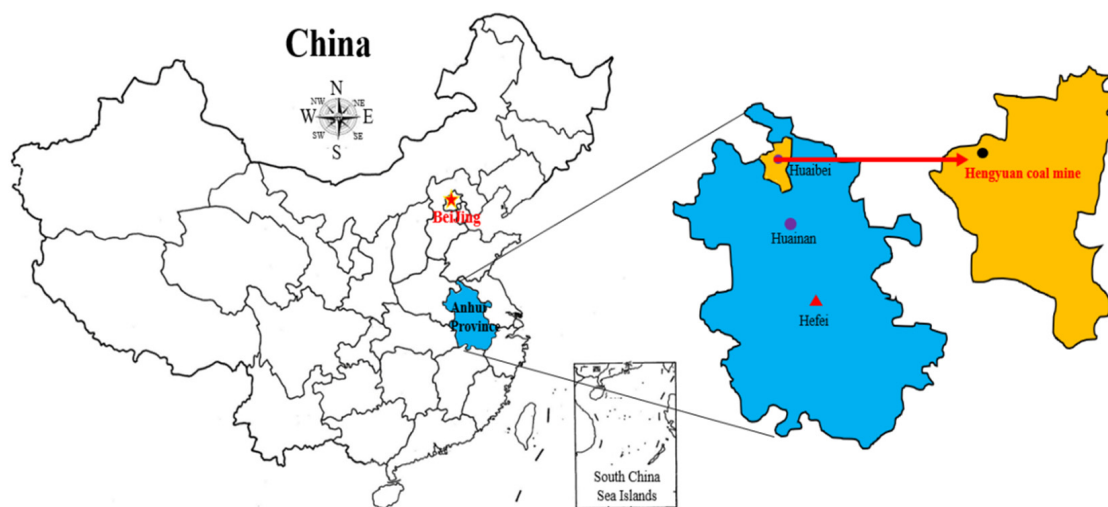

Figure 1. Geographical location map of Hengyuan coal mine.

The II633 working face is the second working face prepared for mining area II63. The whole working face is located in the footwall of the Mengkou reverse fault. The main mining seam is the #6 coal seam, which is located in the middle of the Shanxi formation. The coal seam structure is simple, mainly a single coal seam, with a layer of mudstone mixed with gangue locally. It is a relatively stable coal seam. The thickness of the coal seam is 0.55~5.93 m, with an average of 2.93 m, the dip angle of the coal seam is 10~25°, with an average of 10°, and the buried depth elevation of the coal seam is −655~−778 m. It is designed as a fully–mechanized mining face. Generally, it can be characterized as near–strike longwall mining. The strike length of the working face is 2058 m, and the inclined width is 182 m. According to the drilling data of the working face, the roof of the #6 coal seam is mainly mudstone, followed by siltstone, with a small amount of sandstone, 39~70 m away from the aluminum mudstone, with an average of 55.5 m. The drilling of

working face II633 revealed that the lithology between the floor of the #6 coal seam and the ash roof of the Taiyuan formation is mainly mudstone and siltstone, mixed with 1~2 layers of sandstone, with sand mudstone interbedding locally, and the lithology is relatively dense. There are 86 Taihui boreholes in the Hengyuan coal mine. According to statistics, there are 83 boreholes with limestone in the #6 coal mines. Six boreholes are affected by faults, and their spacing becomes thinner, ranging from 25.10 m to 37.44 m. Under normal conditions, the spacing is 42.50~69.82 m, and the average spacing is 53.70 m. From the above data, it can be seen that, in general, when mining the #6 coal seams, the floor rock layer of this section can play a role in water separation.

2.2. Hydrology of Study Area Overview

A total of 86 limestone boreholes in the Taiyuan formation can be found in the Hengyuan coal mine. Only eight holes of water expose the whole formation of the Taiyuan formation, the rest only expose 1~4 ash, and the 05—3 hole exposes 10~12 ash. The total thickness of the whole group is 115.55 m, and it is composed of limestone, mudstone, siltstone, and thin coal seams, of which limestone is the main one. The thickness of the 12 layers of limestone is 53.87 m, accounting for 46.6% of the total thickness of the whole group. Underground, the confined water is mainly stored and transported in the limestone karst fissure network. The water abundance mainly depends on the degree of karst fissure development. The development of the karst fissures is uneven, so the water abundance is also uneven. The karst fissures develop with rich water content and sufficient recharge from water sources, meaning they are not easy to drain. The water level elevation is 30.28 m, the unit displacement $q = 0.704 \sim 3.15$ L/s.m, the permeability coefficient is about 1.77 m/d, the hydrochemistry type is SO_4—Na.Ca, the mineralization degree is 3.50 g/L, and the water pressure of the Taiyuan Formation limestone is 3.85~5.38 MPa. The limestone karst water of the Taiyuan formation is a floor aquifer that poses the greatest threat to the II633 working face. The lithology of the surrounding rock of the top and floor of the working face is shown in Figure 2.
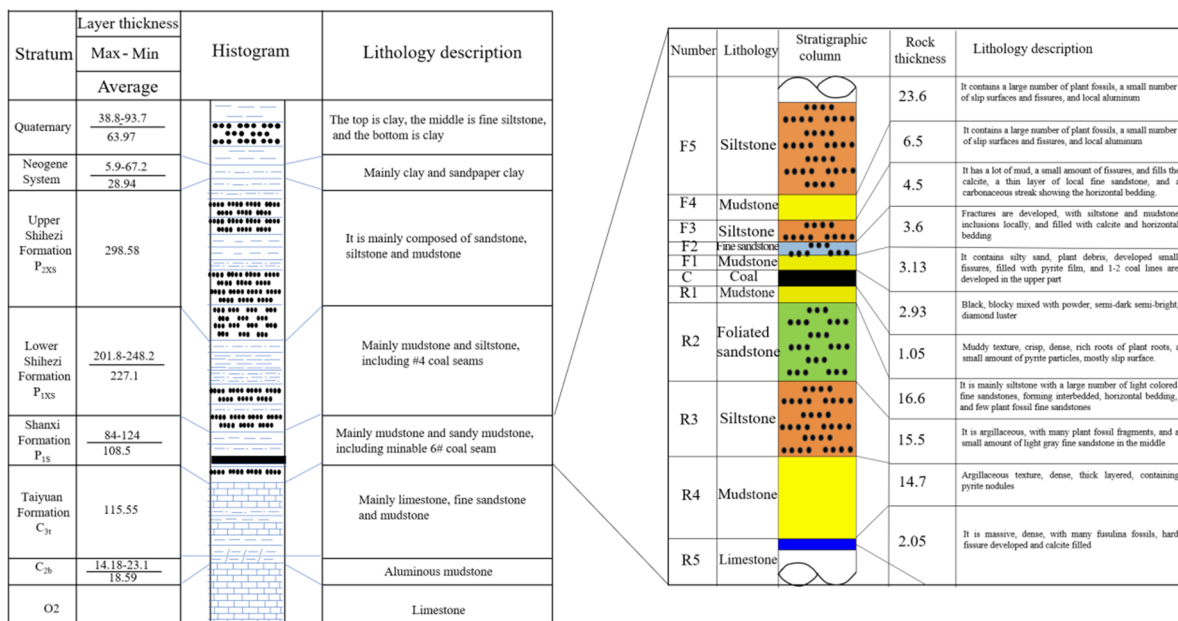
Figure 2. #6 coal roof and floor rock stratum histogram.

3. Theoretical Analysis and Calculation of the Damage Depth of the Floor

When mining under deep confined water conditions, the floor is not only affected by mining stress its failure mechanism is also more complex. Therefore, the coupling effect of mining disturbance and the confined water should be considered when analyzing the damage characteristics of the floor aquiclude above the confined water. The stress state at

any point of the coal seam floor can be regarded as the superposition of the original rock stress and the additional stress. The original rock stress increases linearly with the extension of the buried depth, which can be estimated approximately according to the formula $P = \gamma H$ (γ is the average unit weight of the overlying strata, and H is the average buried depth of the coal seam). Therefore, the stress characteristics at any point of the floor depend critically on the additional stress solution. In addition, because the floor rock stratum is composed of several or more rock masses with different lithology and is distributed in layered sedimentation, and because the physical properties of each rock stratum are anisotropic in the longitudinal direction, the floor aquiclude can be regarded as a semi–infinite body model. With reference to the mine pressure and rock stratum control theory, the stress state and distribution law of the floor after coal seam recovery are shown in Figure 3. It can be seen from the figure that the thickness of the aquifer on the floor of the coal seam is $h_1 + h_2 + h_3$. Affected by the mining disturbance of the coal seam and the coupling effect of confined water pressure, the floor is damaged, and there is a dominant channel for confined water diversion. The thickness of the mining failure zone of the floor is h_1, and the thickness of the confined water diversion zone is h_3. At this time, the thickness of the rock layer mainly responsible for the water barrier task of the floor is h_2, so this section of the rock layer will become a key water barrier layer [34,35].
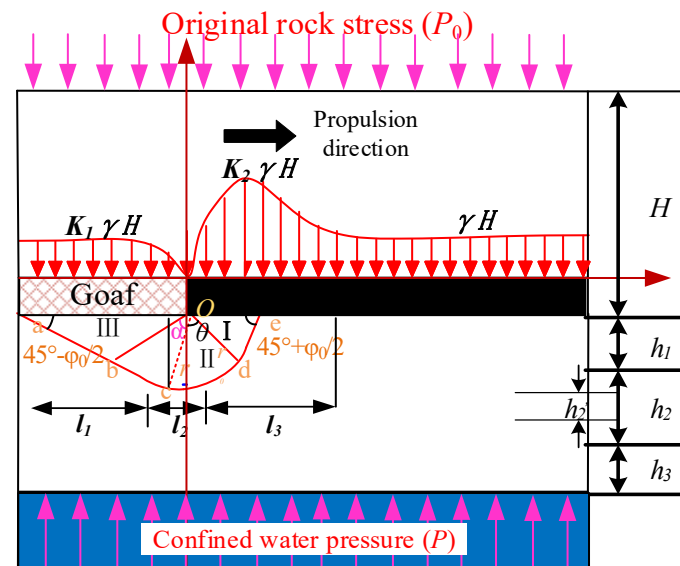

Figure 3. Stress characteristics of the floor after coal mining.

3.1. Plasticity Theory Formula to Calculate the Depth of Damage of the Floor

Coal mining has greatly disturbed the original stress state of the floor. In order to prevent and control water inrush disasters on the floor, it is very important to study and predict the damage depth of the floor. When the coal seam is not excavated, the floor is in an elastic state, and when the mining stress exceeds the ultimate yield strength of the floor rock stratum, the floor rock stratum will undergo plastic deformation and failure [36,37]. According to the plastic theory, the plastic failure area of the floor aquiclude under the influence of mining can be divided into three areas according to the distribution of mining stress: the active stress area of the coal seam floor (I), the deformation transition area of the floor (II), the passive stress area of the floor failure (III). In the three plastic deformation areas, the slip line (boundary line of plastic area) of areas I and III is approximately a straight line, while the deformation and failure slip line of the coal seam floor in area II is in the shape of logarithmic spiral bending, and its expression is:

$$r = r_0 \exp(\theta \tan \varphi_0) \tag{1}$$

where: r is the distance between Oc, m; r_0 is the distance between Od, m; φ_0 is the internal friction angle of the floor rock formation, (°); θ is the included angle between r and r_0, (°).

Assuming that the maximum destruction depth of the floor is D, the analysis of the above figure shows that the destruction depth of the floor D is:

$$D = r \sin \alpha \tag{2}$$

Bring Formula (1) into Formula (2), and the maximum damage depth of the floor is:

$$D = r_0 \exp(\theta \tan \varphi_0) \sin \alpha \tag{3}$$

$$r_0 = \frac{l_3}{2 \cos\left(\frac{\pi}{4} + \frac{\varphi_0}{2}\right)} \tag{4}$$

$$\alpha = \frac{\pi}{2} - \theta + \left(\frac{\pi}{4} - \frac{\varphi_0}{2}\right) \tag{5}$$

Substituting Formulas (4) and (5) into Formula (3), we can find:

$$D = r_0 \exp(\theta \tan \varphi_0) \cos\left(\theta + \frac{\varphi_0}{2} - \frac{\pi}{4}\right) \tag{6}$$

While $\frac{dD}{d\theta} = 0$, the development depth of the plastic zone of the floor is the largest, i.e.:

$$D_{\max} = \frac{l_3 \cos \varphi_0}{2 \cos\left(\frac{\pi}{4} + \frac{\varphi_0}{2}\right)} \exp\left[\left(\frac{\pi}{4} + \frac{\varphi_0}{2}\right) \tan \varphi_0\right] \tag{7}$$

where: l_3 is the range of coal seam plastic zone.

According to the field measurement research, when the physical and mechanical strength of the roof and floor of the coal seam is higher than that of the coal body, the yield length l_3 of the coal body in the process of coal seam mining is:

$$l_3 = \frac{M}{F} \ln(10\gamma H) \tag{8}$$

$$F = \frac{K_1 - 1}{\sqrt{K_1}} + \left(\frac{K_1 - 1}{\sqrt{K_1}}\right)^2 \arctan \sqrt{K_1} \tag{9}$$

$$K_1 = \frac{1 + \sin \varphi}{1 - \sin \varphi} \tag{10}$$

where: H is the buried depth of the coal seam, m; M is the mining height, m; φ is the internal friction angle of the coal seam, (°).

Combined with the actual physical and mechanical parameters of the #6 coal seam in the Hengyuan coal mine, the average thickness of the coal seam is taken as 2.93 m, the average internal friction angle of the floor rock is taken as 52°, the internal friction angle of the coal seam is 28°, and the average buried depth of the coal seam is taken as 760 m. The average unit weight of the floor rock is $\gamma = 25\,kN/m^3$, substituted into Formulas (7)–(10), and the maximum depth of the plastic zone of the floor is:

$$D_{\max} = \frac{6.87 \times \cos 52°}{2 \cos\left(45° + \frac{52°}{2}\right)} \times \exp\left[\left(\frac{\pi}{4} + \frac{52°}{2} \times \frac{\pi}{180}\right) \times \tan 52°\right] = 31.73\text{m}$$

3.2. Analysis of the Risk of Water Inrush in the Floor

The coefficient of water inrush [38], which is the ratio of the confined water pressure on the floor of the working face to the thickness of the floor aquiclude, has been further optimized by many scholars, considering the influence of the floor damage depth on the

water barrier performance of the floor with the in–depth research on the risk of water inrush from the floor [39].

$$T = \frac{P}{h - h_1} \tag{11}$$

where P is the confined water pressure on the floor, MPa; h is the thickness of the floor aquiclude, m; h_1 is the depth of damage to the floor under the influence of mining, m.

From the theoretical analysis, the damage depth of the floor of the II633 working face of the Hengyuan coal mine is 31.73 m. The average distance from the floor of the #6 coal to the roof of the Tai ash confined—water—bearing layer is 53.87 m, so the thickness of the key stratum of aquiclude h_2 is 22.14 m. In addition, according to the revealed hydrogeological data, there are sufficient water sources for recharging the confined water in the floor of the working face, and there is strong heterogeneity, and the water pressure is calculated according to the maximum water pressure of 5.38 MPa. The final calculated water inrush T of the floor is 0.24 MPa/m, which is much higher than the critical value T_s for water breakout in the Huaibei coalfield (the specified critical value of 0.1 MPa/m for intact floor water inrush and 0.06 MPa/m for non—intact floor water inrush), so the floor of the II633 working face will be threatened by significant confined water during the mining process.

4. Slurry Material Proportioning Test

The above study shows that the floor of working face II633 is damaged to a greater depth under the influence of mining disturbance and the coupling effect of the confined water. The confined water is likely to break through the key stratum of the aquiclude through the confined water conduction zone and conduct with the mining damage zone, which will cause a floor water inrush accident, and the risk of floor water inrush is large. For this reason, the coal seam floor needs to be reinforced by grouting to reduce the depth of damage to the floor and to reduce the risk of water inrush from the floor. To achieve the ideal grouting effect, in addition to the excellent grouting process, the ratio and performance of the slurry material are also crucial to the grouting effect. In this section, bentonite, a water–reducing agent, and sodium silicate were selected as slurry additives, the water cement ratio, viscosity, setting time, and compressive strength of the slurry were used as slurry performance evaluation indexes, and a single factor test was adopted to determine the optimal selection range of the slurry content, and the response surface optimization analysis method was adopted to determine the optimal value of each index.

4.1. Selection of Grouting Materials and Performance Index

The research found that bentonite can improve the water separating proportion of the cement slurry and improve the stability of the slurry, the water–reducing agent can reduce the viscosity of the cement slurry and improve the plasticity of the cement slurry, and sodium silicate can effectively shorten the setting time of the cement slurry. Therefore, this paper drew on the experience of road construction, mixed the above–mentioned materials into the grouting materials, and achieved the purpose of ensuring the grouting effect, reducing the cost of grouting, and increasing the profit of tons of coal by optimizing the ratio of each material.

(1)   Bentonite properties

Bentonite is a yellow–green clay that is easy to swell for paste after adding water; it has a low permeability and can effectively improve the slurry water separating proportion. Its main component is montmorillonite (80~90%), and the PH value is between 8.9 and 10, containing more active metal cations such as Cu^{2+}, Mg^{2+}, Na^+, and K^+, etc., and has superior ion exchange properties.

According to the interlayer cations, bentonite can be classified into Na–bentonite, calcium–based bentonite, hydrogen–based bentonite, and organic bentonite. Na–bentonite was selected for this experiment, and its physical parameters are shown in Table 1.

Table 1. Parameters of Na–bentonite [40].

Density (g/m³)	Liquid Limit (%)	Plastic Limit (%)	Plasticity Index (%)	Particle Composition		
				<0.02	0.02~0.05	0.05~1
2.77	35.5	35.5	45.5	68%	11%	21%

(2)   Water–reducing agent properties

The water–reducing agent is an anionic surfactant, and it can interact with the cations in the cement hydration products; the reaction product is cross–linked adsorbed on the surface of the cement particles within a certain period of time to hinder or destroy the adsorption cohesion between the cement particles. The selected high–efficiency water–reducing agent from the naphthalene series water–reducing agent has the appearance of a yellow to dark brown powder and is easily soluble in water. Adding a water–reducing agent to concrete can not only increase the strength but also improve its wear resistance, corrosion resistance, and resistance to permeability; its physical properties are shown in Table 2.

Table 2. Physical parameters of naphthalene series water–reducing agent [41].

Density (g/m³)	Solids Content/%	Water Reduction Rate/%	PH Value	Cl– Content/%	Na_2SO_4 Content/%	Total Alkali Quantity/%
1.007	38.4	28.0	6.0	0.1	0.5	0.5

(3)   Sodium silicate properties

Sodium silicate, a soluble inorganic silicate, is an aqueous solution of sodium silicate (chemical formula $Na_2O \cdot nSiO_2$), which is widely used as a mining binder. For the cement slurry with sodium silicate, sodium silicate has a catalytic effect on cement hydration, the cement slurry contains calcium hydroxide, and sodium silicate reacts with it to generate hydrated calcium silicate (hydrated calcium silicate is a kind of cementitious body, and it has high strength) while consuming a certain amount of calcium hydroxide so that its content cannot reach saturation, thus accelerating the hydration of calcium silicate, improving the initial setting time of the cement slurry and increasing the early compressive strength of the grouting stone body. In addition, the charge carried by the slurry colloid is opposite to the charge carried by the sodium silicate, and the two have opposite electrical properties, which can effectively improve the setting speed of the slurry after the neutralization and condensation of the colloidal particles.

4.2. Slurry Performance Index Test

The performance indexes of the slurry injection slurry for water plugging and reinforcing the floor rock, excluding the cost of slurry injection, also need to consider the performance indexes of the slurry itself, including the slurry water separating proportion, viscosity, setting time, and the compressive strength of the grouting stone body [42].

(1)   Determination of slurry water separating proportion

The slurry water separating proportion refers to the volume ratio of water separation from the slurry at rest due to the natural settlement of cement particles by gravity, which is one of the important indicators to measure the stability of the slurry and the degree of fracture filling. To determine the water separating proportion, the configuration of the slurry poured into the cylinder, the liquid level, and the 1000 mL scale value flush, the mouth of the cylinder was sealed, placed on the horizontal table, and rested for 3 h for every 10 mine observation and the data were recorded; three consecutive readings of the same can be identified as the slurry was completely water separated to achieve stability.

When testing another slurry water separating proportion, the cylinder should be cleaned and kept dry inside.

(2)   Slurry viscosity measurement

The slurry viscosity is a physical quantity that measures the internal friction of a slurry as it flows, and it represents the rheology and injectability of the slurry. In this experiment, a funnel viscometer was selected for the viscosity determination by the time required for a unit volume of the slurry to flow out of the lower port of the funnel.

(3)   Slurry setting time measurement

For the slurry setting time for each slurry admixture hydration reaction time required, there is an initial setting, a final setting time, and the test selection of the Vicat instrument for slurry setting time determination. For the determination of the initial setting time when the initial setting needle from the bottom of the test mold 4 mm ± 1 mm can be for the slurry beginning the initial setting. For the determination of the final setting time, the final setting needle and then the test mold surface does not leave a ring–shaped imprint shall prevail.

(4)   Determination of the compressive strength of the grouting stone body

The slurry condensed to form a stone body, and the compressive strength is the stone strength, which visually reflects the bearing capacity of the reinforced rock formation. The mixed slurry with different admixture ratios was poured into a standard mold of 50 mm × 100 mm to make standard specimens, and after the time condensation and demolding, it was placed into a standard curing box and cured for 7 d and 28 d, respectively, to test the compressive strength of the specimens. Each slurry performance index measurement test is shown in Figure 4.
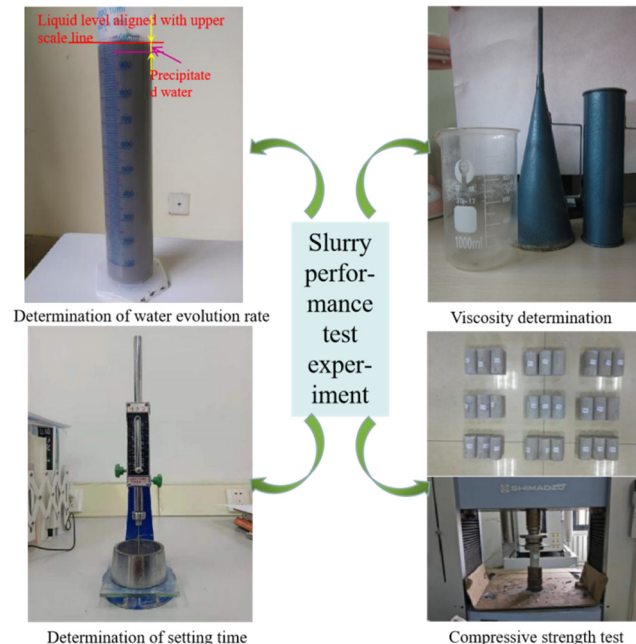
Figure 4. Slurry performance index test experiment.

4.3. Single–Factor Experimental Design and Result Analysis of Grouting Material Proportioning

(1)   The effect of single admixture addition on slurry performance

(a)   The effect of different water–cement ratio on slurry performance

According to the «Specification of mine curtain grouting» [43–45], the water–cement ratios selected for this single–factor experiment ranged from 0.5, 0.6, 0.8, 1.0, and 2.0. After the slurry was completely mixed, the water separating proportion, viscosity, setting time,

and compressive strength of the grouting stone body of the slurry were measured under different water–cement ratios, and the test results are shown in Figure 5.

Figure 5. Performance index of slurry with different water–cement ratio. (**a**) water separating proportion; (**b**) comprehensive performance indicators.

From the analysis of Figure 5, it can be seen that: in the water separating proportion, the slurry water separating proportion is closely related to the w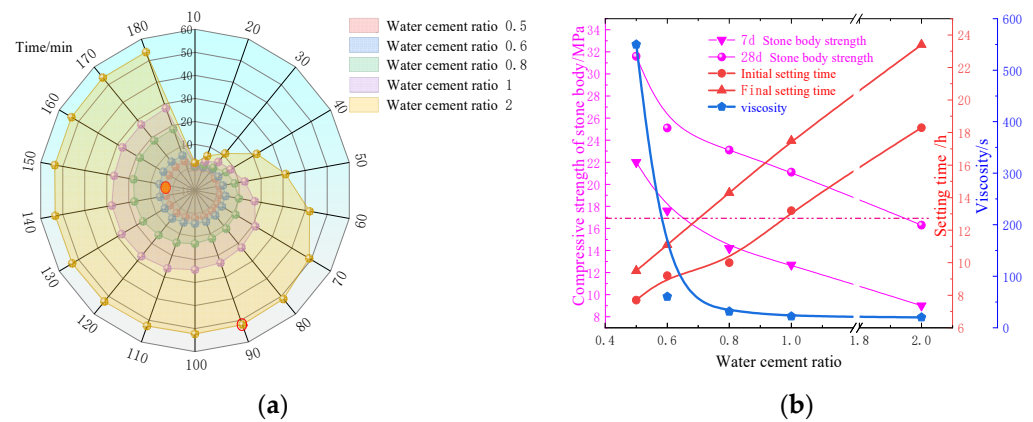ater–cement ratio. The greater the water–cement ratio, the faster the slurry water separation and the greater the water separating proportion, and when the water–cement ratio is 0.6, the slurry water separating proportion is stable at 6.1% at 150 min, while the water–cement ratio is 2.0, the slurry water separating proportion is stable at 52% at 90 min, the slurry performance is greatly reduced. In terms of viscosity, the viscosity of slurry decreases with the increase in the water–cement ratio value, and they are negatively correlated; the viscosity decrease values are 489.6 s, 28.8 s, 9.5 s, and 1.9 s during the increase in the water–cement ratio from 0.5 to 2.0, the viscosity decrease values are 489.6 s, 28.8 s, 9.5 s, and 1.9 s. When the water–cement ratio value increases from 0.6 to 0.8, the viscosity decrease is larger, i.e., the slurry is less liquid and unfavorable for grouting when the water–cement ratio is larger. In terms of setting time, the trend of the initial and final setting time of the slurry is that the setting time gradually increases with the increase in the water–cement ratio, and when the water–cement ratio is 2.0, the final setting time can reach 23.4 h. This is because the larger the water–cement ratio, the freer the water in the slurry, and the greater the effect of dissolving and dispersing the colloid and crystal of the slurry after hydration, which directly leads to the longer setting time of the slurry; in terms of compressive strength of the grouting stone body, its overall trend when the water–cement ratio is 2.0, the compressive strength of the grouting stone body at 28d is only 16.3 MPa, which is lower than the standard of compressive strength of the grouting stone body not less than 17 MPa required in the grouting project, because the larger the water–cement ratio, the freer the water in the slurry, and the water evaporates after the slurry solidifies, the stone body will form microscopic pores inside the slurry. The freer the water, the greater the porosity, which seriously affects the compressive strength of the grouting stone body. Therefore, the water–cement ratio can be selected from 0.6–1.0.

(b)　　Influence of bentonite dosing on slurry performance

To study the effect of bentonite dosing on the slurry performance, the fixed water–cement ratio was 0.8, the water–reducing agent and sodium silicate dosing were 0.4% and 1%, respectively, and the bentonite dosing was set at four gradients of 1%, 2%, 3%, and 4%. It is necessary to soak the bentonite and water in the container in a ratio of 1:1 for more than 48 h to produce flocculation. The water separating proportion, viscosity, coagulation time, and compressive strength of the grouting stone body of the slurry under different bentonite doping were measured separately, and the experimental results are shown in Figure 6.
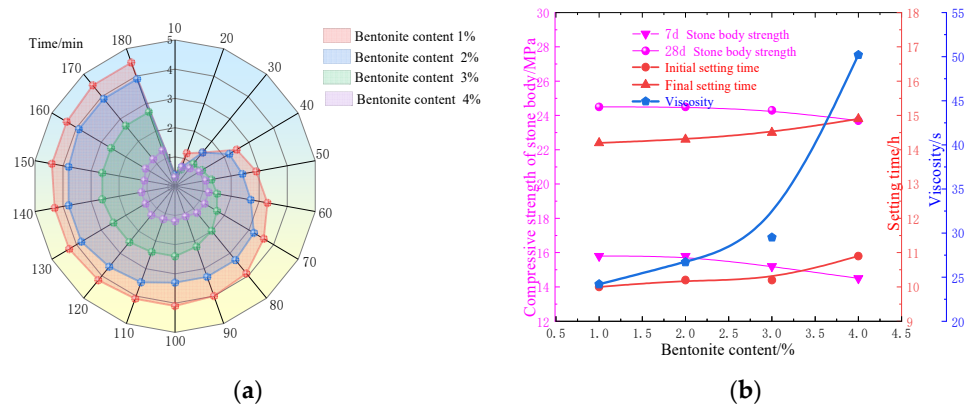
Figure 6. Performance index of slurry with different bentonite dosing. (**a**) water separating proportion; (**b**) comprehensive performance indicators.

The analysis from Figure 6 can be obtained: in the water separating proportion, the greater the amount of bentonite, the slurry water separating proportion reduction trend, the better the stability of the slurry, and all within 80 min water separation stability, that is, bentonite can significantly inhibit the slurry water separating proportion. In the slurry viscosity, the greater the bentonite doping, the greater the viscosity of the slurry, dosing from 1% to 3%, the viscosity of the slurry from 24.2 s to 29.5 s, an increase of 5.36 s, and from 3% to 4%, the viscosity of the slurry from 29.5 s to 50.2 s, and an increase of 20.7 s, which is due to the high concentration of Na^+ in the slurry, can be to due the large number of anions it combined with. The moisture absorption effect is obvious, but the slurry viscosity required in the grouting project needs to be less than 40 s, so bentonite dosing does not take 4%; in the setting time and compressive strength of the grouting stone body, bentonite dosing on the initial setting of the slurry, the final setting time has a certain delayed effect, while the strength after 7 d, 28 d maintenance is slightly weakened, but from an overall view, bentonite dosing on the two slurry performance indicators has very little effect, in the project can be ignored, so the bentonite dosing range is 1–3%.

(c)   The effect of water–reducing agent admixture on slurry performance

In order to study the effect of water–reducing agent dosing on the slurry performance, the water–cement ratio was fixed at 0.8, the dosing of bentonite and sodium silicate were fixed at 1%, and the water–reducing agent dosing was set at five gradients of 0.2%, 0.4%, 0.6%, 0.8%, and 1.0%. When the slurry was stabilized, the water separating proportion, viscosity, setting time, and compressive strength of the grouting stone body of the slurry were measured under different water–reducing agent doses, and the experimental results are shown in Figure 7.
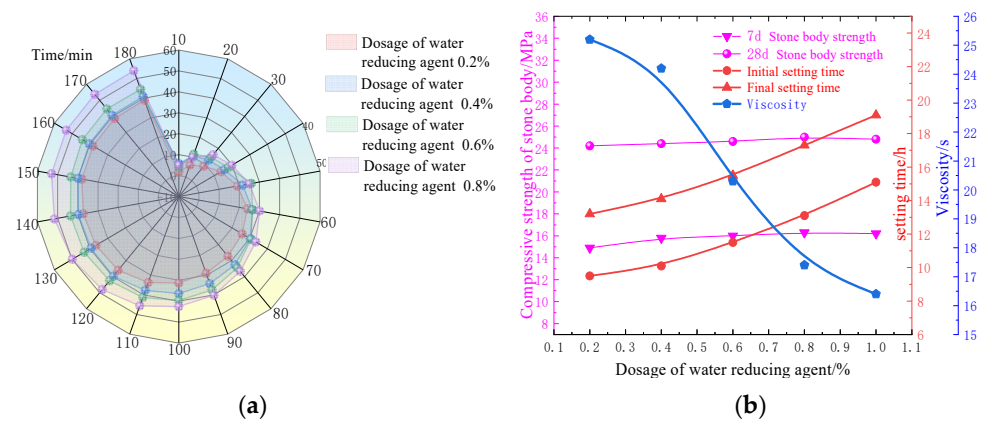

Figure 7. Performance index of slurry with different water–reducing agent dosing. (**a**) water separating proportion; (**b**) comprehensive performance indicators.

From the analysis of Figure 7, it can be obtained that: in the water separating proportion, when the water–reducing agent is mixed in the range of 0.2% to 0.8%, the water separating proportion of the slurry increases with the increase in water–reducing agent, and when the water–reducing agent is mixed at 1%, the slurry does not separate water but appears stratified, which is due to the dispersing effect of water–reducing agent on cement hydrate, prompting the dispersion of large and small particles in the slurry, the larger particles sink to the bottom, while the smaller slurry particles are suspended in the upper layer. In terms of slurry viscosity, the viscosity does not change much when the water–reducing agent dosing is 0.2–0.4%, but when the dosing is increased from 0.4% to 0.8%, the viscosity decreases from 24.2 s to 17.4 s, with a decrease rate of 6.8 s. The reduction rate is faster, and the viscosity reduction effect of the water–reducing agent is obvious. In terms of setting time, the water–reducing agent has an inhibiting effect on setting time, especially when the dosing is greater than 0.4%, and the reason for the inhibitory effect is that the anion of the water–reducing agent dissolved in water combined with cement particles to form a thin film layer, which hinders the adsorption and coagulation between the particles. In terms of the compressive strength of the grouting stone body, different water–reducing agents have little effect on the compressive strength of the grouting stone body of the slurry. To sum up, the selection range of water–reducing agent dosing is 0.4–0.8%.

(d)   The effect of sodium silicate admixture on slurry performance

In order to study the effect of water–glass dosing on the slurry performance, the water–cement ratio was fixed at 0.8, the dosing of bentonite and water–reducing agent were fixed at 1% and 0.4%, respectively, and the water–glass dosing was set at four gradients of 1%, 2%, 3%, and 4%. When the slurry was stabilized, the water separating proportion, viscosity, setting time, and compressive strength of the grouting stone body of the slurry were measured under different sodium silicate dosing, and the visual graph of the experimental results is shown in Figure 8.
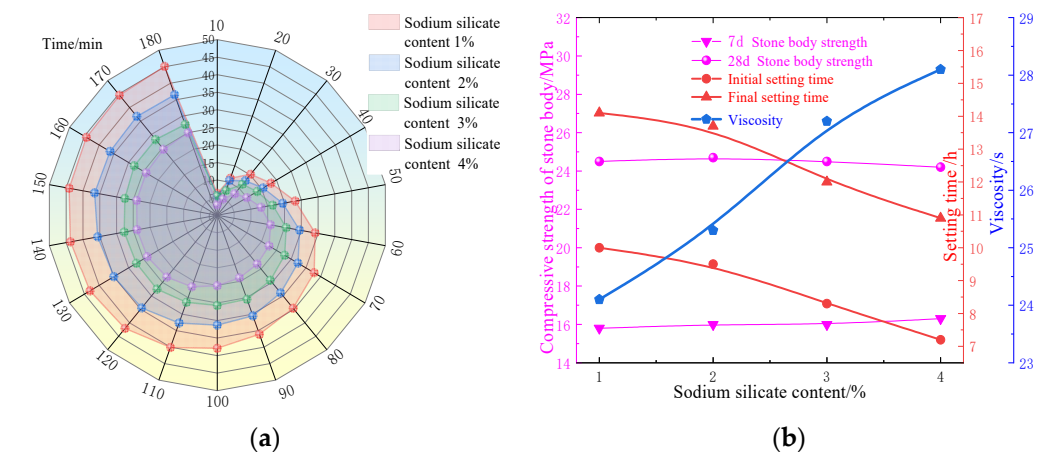
Figure 8. Performance index of slurry with different sodium silicate dosing. (**a**) water separating proportion; (**b**) comprehensive performance indicators.

The analysis from Figure 8 can be obtained: in the water separating proportion, the sodium silicate dosing for the slurry water separating proportion has a significant inhibitory effect; the greater the sodium silicate dosing, the smaller the slurry water separating proportion, the drop gradually decreases, and the drops between the different gradients were 10%, 9%, and 2.5%. The viscosity of the slurry is positively correlated with the amount of sodium silicate; when the amount of sodium silicate is increased from 1% to 4%, the viscosity increases from 24.1 s to 28.1 s, and the increase range is 4 s. In terms of setting time, the water–reducing agent can promote the setting of the slurry, and with the increase in the amount of sodium silicate, the initial and final setting time of the slurry is gradually shortened. In terms of the compressive strength of the grouting stone body, the amount

of sodium silicate has a small effect on the strength of the stone body; in summary, it is determined that the selection range of sodium silicate admixture is 1–3%.

4.4. Response Surface Experimental Design of Slurry Proportioning Based on CRITIC Weighting Method

Based on the single–factor experiments affecting the slurry performance, it is also necessary to clarify the interaction relationships among the influencing factors, for which a response surface test design is adopted in this paper to optimize the proportion of grouting materials. The response surface test can determine the correlation between the factors and the corresponding regression equation within a certain test range. Considering the two–by–two interaction between the different influencing factors and single–factor quadratic term influence, this test adopts the second–order response surface model and designs a four–factor, three–level test, and the setup results are shown in Table 3.

Table 3. Experimental factor codes.

Code	Water–Cement Ratio	Bentonite (%)	Water–Reducing Agent (%)	Sodium Silicate (%)
−1	0.6	1	0.4	1
0	0.8	2	0.6	2
1	1.0	3	0.8	3

The specific experimental design method was a response surface analysis design using the water–cement ratio (A), bentonite (B), water–reducing agent (C), and sodium silicate (D) as response factors. The Box–Behnken test method in the Design expert software was used to analyze the response to the combined scores of the water separating proportion, viscosity, setting time, and compressive strength, and the test was divided into 29 groups, including 24 groups of precipitation factor tests and five groups of central tests. The test results are shown in Table 4.

Table 4. Test results.

Serial Number	A	B	C	D	Water Separating Proportion (%)	Viscosity (s)	Setting Time (h)	Compressive Strength (MPa)
1	0.8	2	0.8	3	2.5	26.28	13.14	24.18
2	0.6	3	0.6	2	2.4	28.53	11.01	26.20
3	0.8	2	0.4	3	2.9	28.28	10.01	24.33
4	0.8	3	0.6	3	2.4	19.56	9.02	25.16
5	0.8	1	0.8	2	4.1	19.41	16.20	23.33
6	0.6	2	0.6	3	3.2	28.07	7.27	27.25
7	0.6	2	0.8	2	4.1	20.57	14.54	25.18
8	0.8	2	0.6	2	4.2	16.87	11.59	24.88
9	1.0	2	0.6	3	4.8	18.47	18.08	22.56
10	1.0	3	0.6	2	3.9	18.29	19.80	21.29
11	0.8	2	0.6	2	4.3	16.05	11.15	25.63
12	0.8	3	0.8	2	5.1	17.35	12.28	24.59
13	0.8	2	0.8	1	3.5	19.31	15.24	24.72
14	0.6	1	0.6	2	3.2	26.36	10.27	26.31
15	1.0	2	0.6	1	5.3	24.15	12.48	23.57
16	1.0	2	0.8	2	5.4	18.43	16.49	23.65
17	0.8	3	0.4	2	2.8	24.61	13.58	24.05
18	0.8	1	0.4	2	3.3	25.32	13.43	24.56
19	0.8	1	0.6	3	3.8	21.30	10.10	24.66
20	0.8	3	0.6	1	2.6	23.42	15.46	24.12
21	0.8	1	0.6	1	4.5	20.24	15.24	24.62
22	0.8	2	0.6	2	4.1	16.11	12.12	22.35
23	0.8	2	0.6	2	4.3	16.29	11.42	25.35

Table 4. *Cont.*

Serial Number	A	B	C	D	Water Separating Proportion (%)	Viscosity (s)	Setting Time (h)	Compressive Strength (MPa)
24	0.6	2	0.6	1	4.7	26.13	10.36	26.85
25	1.0	1	0.6	2	5.9	17.51	16.37	21.45
26	0.8	2	0.4	1	2.9	26.72	14.32	24.70
27	1.0	2	0.4	2	4.9	19.80	15.58	21.38
28	0.8	2	0.6	2	4.5	17.29	13.42	27.35
29	0.6	2	0.4	2	3.1	22.50	14.27	23.16

In order to objectively assign weights to each influencing factor, the CRITIC weight method was used in this paper to calculate the influence weights of the water–cement ratio, bentonite dosing, water–reducing agent dosing, and water–glass dosing on slurry performance using the magnitude of data correlation among the factors.

(1)   Standardization and normalization

The different characteristics of the material have different measurement and reflection laws that need to be standardized and normalized. Among them, according to the actual needs of the floor confined water grouting reinforcement project, set the compressive strength of the grouting stone body and viscosity as the positive indicators; that is, the larger the value, the better the setting time and water separating proportion as the inverse indicators; that is, the hope of small characteristics, the different characteristics of the data normalized distribution according to Formulas (12) and (13) calculations.

$$x_{ij}^{\text{grow larger}} = \frac{x_j - x_{\min}}{x_{\max} - x_{\min}} \tag{12}$$

$$x_{ij}^{\text{grow smaller}} = \frac{x_{\max} - x_j}{x_{\max} - x_{\min}} \tag{13}$$

where x_{ij} is the data normalization results; x_j is the amount of indicators tested in the j_{th} group of tests; $x_{\max}$ is the maximum value of the detection amount of each index; and $x_{\min}$ is the minimum value of the detection amount of each index.

(2)   Variability of indicators

In the CRITIC method, the standard deviation is used to indicate the fluctuation of the difference in the values taken within each indicator. The larger the standard deviation indicates a greater difference in the value of the indicator, and more information can be reflected, and the stronger the evaluation intensity of the indicator itself, and more weight should be assigned to the indicator.

$$\begin{cases} x_j = \frac{1}{n}\sum_{i=1}^{n} x_{ij} \\ S_j = \sqrt{\frac{\sum_{i=1}^{n}(x_{ij} - \bar{x}_j)^2}{n-1}} \end{cases} \tag{14}$$

where S_j is the Standard deviation of the j_{th} indicator.

(3)   Conflicting indicators

The stronger the correlation with other indicators, the less conflicting the indicator is with other indicators, the more the same information is reflected, and the more duplication of the evaluation content is reflected, which to some extent also weakens the evaluation strength of the indicator and should reduce the weight assigned to the indicator.

$$R_j = \sum_{i=1}^{p}(1 - r_{ij}) \tag{15}$$

where r_{ij} is the number of indicators tested in the j_{th} group of tests.

(4) Amount of information

$$C_j = S_j \times R_j \tag{16}$$

(5) Objective weights

$$w_i = \frac{C_j}{\sum_{j=1}^{p} C_j} \tag{17}$$

Substituting the test results data in Table 2 into Equations (15)–(20), the values of each evaluation index can be calculated, as shown in Table 5. From Table 5, the weighting of each slurry performance index can be obtained as follows: viscosity > setting time > compressive strength of the grouting stone body > water separating proportion.

Table 5. Results of CRITIC weighting analysis.

Item	Variability of Indicators	Conflicting Indicators	Amount of Information	Objective Weighting
Water separating proportion	0.979	3.568	3.495	0.100
Viscosity	4.119	3.627	14.939	0.427
Setting time	2.848	3.735	10.637	0.304
Compressive strength of the grouting stone body	1.617	3.661	5.919	0.169

In order to obtain the correlation between the evaluation object and the optimal solution, the calculation of the gray correlation coefficient requires setting up a reference sequence and a comparison sequence and performing the calculation of the deviation sequence. The grey correlation coefficient is obtained by taking the water separating proportion, viscosity, setting time, and the compressive strength of the grouting stone body as the comparison sequence and the normalized weighted results of the four indicators as the reference sequence.

$$g_{ij} = \frac{\min_i \min_j |1 - x_{ij}| + \rho \max_i \max_j |1 - x_{ij}|}{|1 - x_{ij}| + \rho \max_i \max_j |1 - x_{ij}|} \tag{18}$$

where ρ is the judgment coefficient defined in (0, 1) is taken to be 0.5.

The gray correlations of each group of tests under different properties were taken as the weighted average, as a quantitative expression of the correlation between the reference and comparison sequences, which is the comprehensive evaluation degree G of the material modification effect, and the larger G indicates the better comprehensive properties of the material. The results of gray correlation values of different properties and CRITIC weighted comprehensive evaluation are shown in Table 6.

$$G_i = \sum_{i=1}^{n} w_i g_{ij} \tag{19}$$

Table 6. Calculation results of gray correlation coefficient and weighted comprehensive evaluation.

Serial Number	Separating Proportion	Viscosity	Setting Time	Compressive Strength	CRITIC Weighted Composite Value
1	0.856	0.486	0.613	0.656	0.589
2	0.725	0.464	0.923	0.635	0.657
3	0.967	0.440	0.960	0.650	0.685
4	0.358	0.457	0.377	0.530	0.434
5	0.708	0.961	0.553	0.956	0.809
6	0.739	0.619	0.487	0.842	0.627
7	0.844	0.877	0.787	1.000	0.865
8	0.664	0.424	0.490	0.560	0.490
9	0.476	0.962	0.417	0.827	0.723
10	0.582	0.823	0.343	0.780	0.644
11	0.592	0.371	0.422	0.511	0.431
12	0.764	0.496	0.618	0.657	0.586
13	0.782	0.709	0.788	0.891	0.769
14	0.849	0.624	0.761	0.786	0.714
15	0.382	0.538	0.649	0.666	0.577
16	0.486	0.840	0.591	0.939	0.743
17	0.708	0.531	0.721	0.712	0.635
18	1.000	0.479	0.682	0.635	0.618
19	0.587	0.667	0.441	0.683	0.592
20	0.638	0.585	0.568	0.715	0.606
21	0.757	0.943	0.755	0.938	0.864
22	0.559	0.402	0.466	0.493	0.451
23	0.472	0.341	0.362	0.465	0.381
24	0.625	0.548	0.669	0.681	0.614
25	0.381	0.913	0.530	0.975	0.752
26	0.992	0.390	0.516	0.533	0.512
27	0.476	0.747	0.527	0.840	0.667
28	0.554	0.381	0.459	0.574	0.453
29	0.757	0.673	0.708	0.845	0.719

4.5. Analysis of Comprehensive Evaluation Results

(1)   Evaluation model establishment

Multiple regressions were fitted to the test data in Table 2; Table 4 using Design expert software to establish a composite score response model. The regression equation for the composite score was:

$$
\begin{aligned}
y = {}& 0.44 - 0.00748x_1 - 0.066x_2 + 0.044x_3 - 0.024x_4 \\
& -0.013x_1x_2 - 0.017x_1x_3 + 0.033x_1x_4 - 0.06x_2x_3 + 0.025x_2x_4 - 0.088x_3x_4 \\
& +0.15x_1{}^2 + 0.1x_2{}^2 + 0.14x_3{}^2 + 0.062x_4{}^2
\end{aligned}
\tag{20}
$$

where y is the composite score response value; x_1 is the water–cement ratio; x_2 is the bentonite dosing; x_3 is the water–reducing agent dosing; and x_4 is the sodium silicate dosing.

The residual normal probability of the model is shown in Figure 9. As can be seen from Figure 9, the test points are distributed on the diagonal and on both sides of the diagonal, and the average deviation of the model is small, indicating that the model is reasonably established and the reliability of the fitted equations is good. The residual results of the prediction model are shown in Figure 10, where the residuals are randomly distributed around zero with no outliers, indicating that the predicted and measured values are in high agreement.
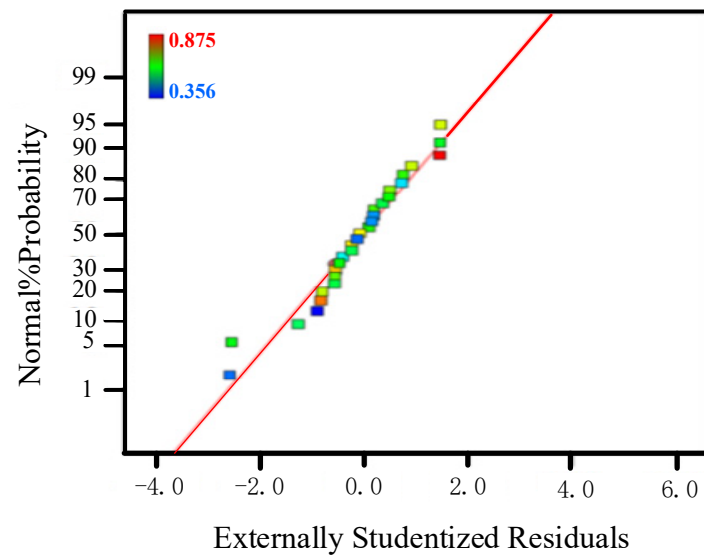
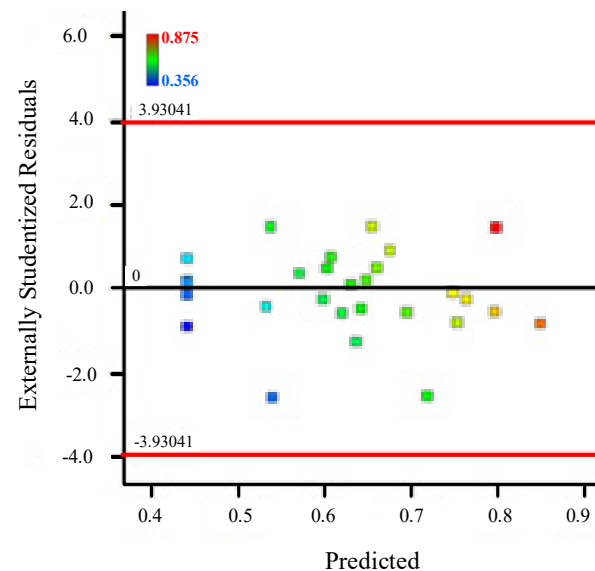**Figure 9.** Normal distribution of residuals.

Figure 10. Residual plot of the prediction model.

The analysis of variance of the regression equation after fitting the prediction model is shown in Table 7. From the analysis in Table 7, it can be concluded that the *p*–value of the model is less than 0.01, and the model is extremely significant and statistically significant. For the four single factors, A, B, C, and D, the main order of influence of the four factors is B > C > D > A; that is, the bentonite admixture has the most significant effect on the slurry performance, the water–reducing agent admixture, sodium silicate admixture, and the water–cement ratio is the second. The misfit terms of the models are all greater than 0.05, the misfit is not significant, the experimental error is small, and the fit with the actual law is high.

Table 7. Analysis of variance of regression equations.

Parameters	Square Sum	Degree of Freedom	Mean Square Error	F	P	Significance
Models	0.3900000	14	0.0280000	4.89	0.0027	**
A	0.0006716	1	0.0006716	0.12	0.7350	
B	0.0520000	1	0.0520000	9.16	0.0091	**
C	0.0230000	1	0.0230000	4.10	0.0625	
D	0.0071030	1	0.0071030	1.26	0.2803	
AB	0.0006490	1	0.0006490	0.12	0.7393	
AC	0.0012170	1	0.0012170	0.22	0.6491	
AD	0.0044770	1	0.0044770	0.80	0.3876	
BC	0.0140000	1	0.0140000	2.57	0.1311	
BD	0.0025690	1	0.0025690	0.46	0.5104	
CD	0.0310000	1	0.0310000	5.53	0.0338	*
A^2	0.1500000	1	0.1500000	26.06	0.0002	**
B^2	0.0670000	1	0.0670000	11.83	0.0040	**
C^2	0.1200000	1	0.1200000	21.75	0.0004	**
D^2	0.0250000	1	0.0250000	4.36	0.0556	
Residual	0.0790000	14	0.0056310			
Misfit error	0.0720000	10	0.0072420	4.51	0.0797	
Absolute error	0.0064180	4	0.0016050			
Total deviation	0.4600000	28				

Note: * is significant ($0.01 < p < 0.05$), ** is extremely significant ($p < 0.01$).

The results of the model credibility analysis are shown in Table 8. As can be seen from Table 8, the correlation coefficient and the modified correlation coefficient of the model are 0.8301 and 0.8603, respectively, which are close to a high degree, indicating that the regression equation is a good fit. The signal-to-noise ratio was 7.566 > 4, while the coefficient of variation was 11.95%, indicating the high precision and credibility of the test.

Table 8. Model plausibility analysis.

Model	Std. Dev	Mean	R^2	Adj-R^2	Pred-R^2	Press	C.V.%	Adeq-Precisior
y	0.0750	0.6300	0.8301	0.8603	0.0797	0.4300	11.9500	7.5660

(2) Two–by–two interaction between factors

The response curve diagram represents the response results with two of the factors constituting the three–dimensional graph, the curvature of the response surface represents the degree of interaction between the factors; the curvature is large, indicating that the interaction between the factors has a greater impact and vice versa indicating that the interaction has a smaller impact. In order to analyze the influence of the interaction between the water–cement ratio, silica powder, and liquid alkali on the comprehensive evaluation of the model, the response surface plot of the influence of the interaction between each factor is drawn as shown in Figure 11.

From the analysis of Figure 11, to determine the optimal ratio of materials: water–cement ratio 0.808, bentonite 2.326%, water–reducing agent 0.568%, sodium silicate 2.197%, modified water–cement ratio, and each grouting material admixture are water–cement ratio 0.8, bentonite 2%, water–reducing agent 0.6%, and sodium silicate 2%.
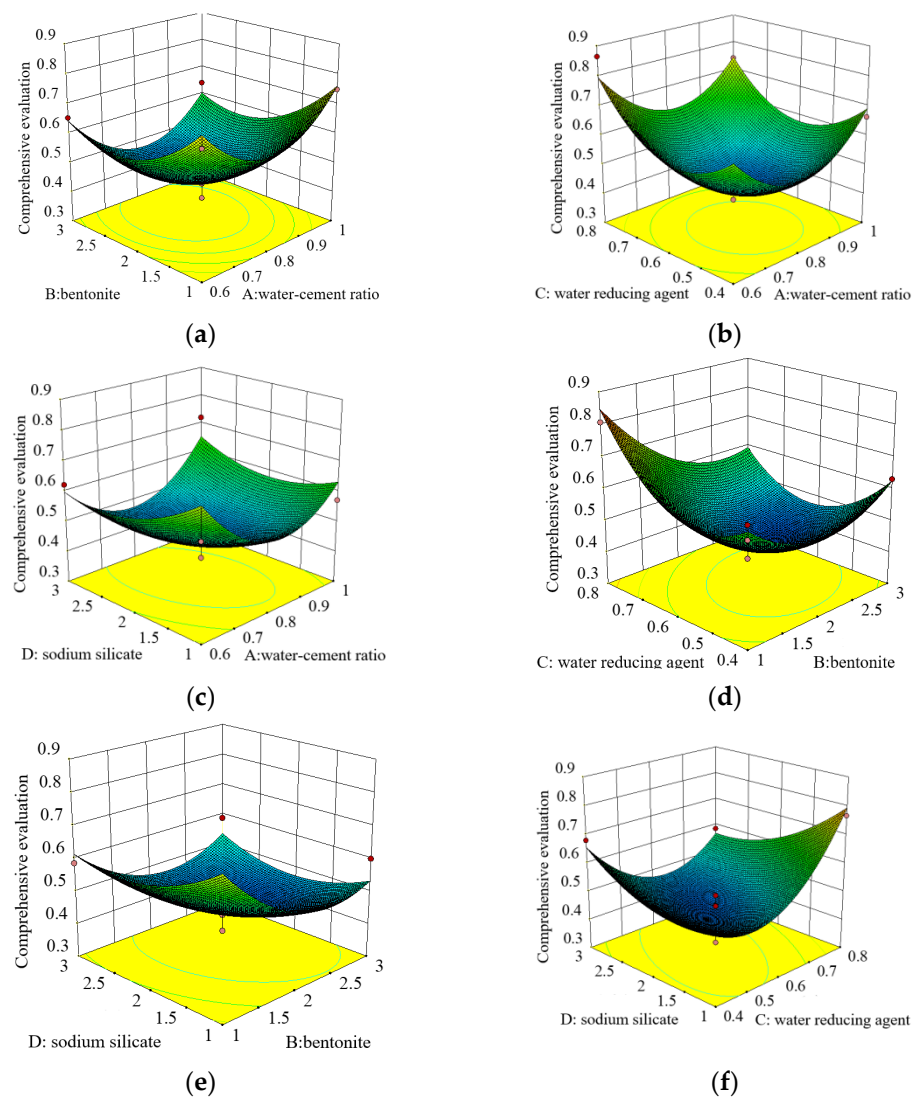
Figure 11. Interaction relationship of effect factors. (**a**) A, B interaction effect; (**b**) A, C interaction effect; (**c**) A, D interaction effect; (**d**) B, C interaction effect; (**e**) B, D interaction effect; (**f**) C, D interaction effect.

5. Field Application

5.1. Subgrade Damage Depth Strain Method Monitoring

In order to test the slurry performance and grouting effect, the dynamic law of pre–mining and post–mining deformation of the coal seam floor and the law of mineral pressure manifestation were analyzed and studied by using the in situ strain method in the field. The method included opening a 3 m × 3 m × 3 m #10 drill field in the machine road of the II633 working face, drilling floor plate monitoring holes in the drill field, and burying strain sensors at different depths. The degree of rock deformation on the floor was analyzed by the strains of the sensors at different measurement point positions on the floor, from which the depth of damage to the floor was further determined and compared with the theoretically calculated value of the depth of damage to the floor to detect the effect of slurry proportioning. The technical parameters of the drilling holes are shown in Table 9.

Table 9. Technical parameters of each sensor.

Hole Number	Angle/(°)	Installation Number	Observation Cable Length/(m)	Vertical Depth of Cable Hole/(m)	Sensitivity/($\mu\varepsilon$/F)
JT10–1	−75°	JT10–1–1	137	25.5	0.3987
		JT10–1–2	134	22.5	0.3963
		JT10–1–3	131	19.5	0.4051
JT10–2	−60°	JT10–2–1	138	29.1	0.4057
		JT10–2–2	135	26.1	0.4006
		JT10–2–3	132	23.1	0.3998
JT10–3	−40°	JT10–3–1	142	34.0	0.3992
		JT10–3–2	139	28.0	0.3962

The GDA1801(4) vibrating string acquisition module and the VWS vibrating string strain gauge were selected to monitor the damage to the floor during coal seam mining, and the acquisition module and the vibrating string strain gauge are shown in Figure 12.
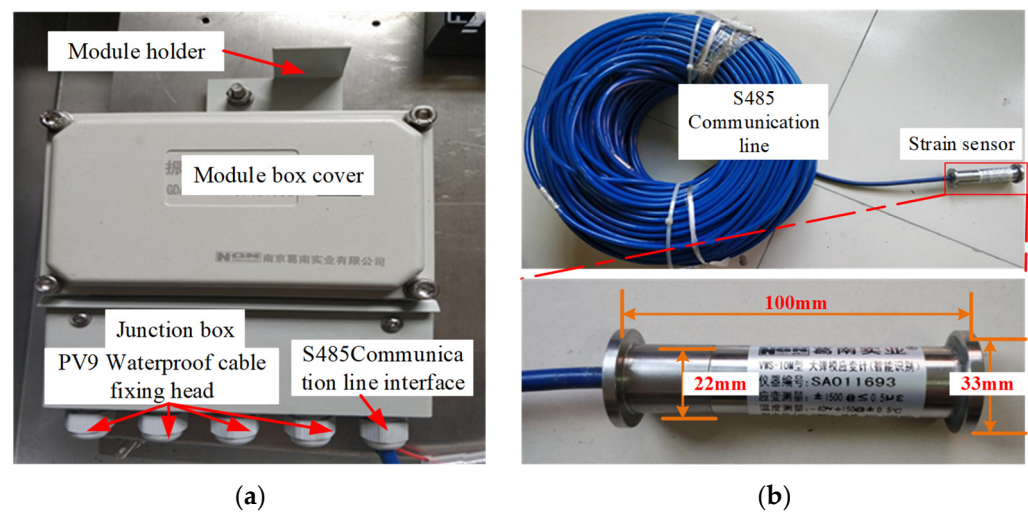

(**a**)   (**b**)

Figure 12. Substrate strain monitoring instrument. (**a**) GDA1801(4) type Vibrioses Acquisition Module; (**b**) VWS Type Vibrioses Strain Gauge.

In order to accurately place the sensor in the borehole and fix it in the preset mounting position without sliding (or reducing the offset), a homemade strain gauge mounting tool was used, with the feeding tool synchronized in the shape of a "Luoyang shovel", and the subsequent mounting rod was a removable mounting rod, as shown in Figure 13. In order to fix the sensor in the borehole without sliding, a homemade sensor positioning module was made, which consisted of two semi–cylindrical modules and four steel pins. A steel pin with a length of 45 mm was inserted around the circular module (diameter of 45 mm) at 90° intervals and bent at an angle (calculated to be 120°) so that the distance between the module and the plane of the pin was 78 mm, making it slightly larger than the diameter of the orifice 75 mm, which allowed the module to better fix the sensor position; in addition, the steel pin was bent at 120° to form a "barbed" shape, which served to fix the sensor at the preset position. In addition, the steel pin was bent 120° to form a "barb", which was used to prevent the sensor from being taken out when the mounting rod was pulled outward after the sensor was installed in the preset position. The positioning module is shown in Figure 14.
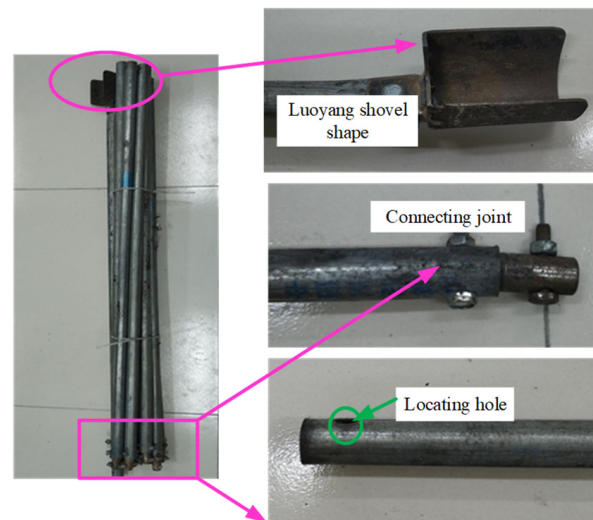
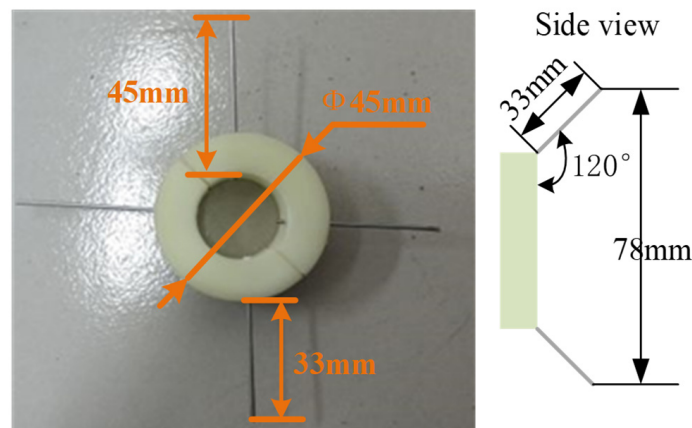**Figure 13.** Strain gauge mounting rod.

Figure 14. Sensor positioning module.

When feeding the sensor into the preset position in the borehole, the sensor head was first placed into the head of the first mounting rod, "Loyang shovel", and the sensor position was fixed using a homemade circular module for fixing the sensor position. Afterward, the sensor was fed into the borehole, then the mounting rods were connected in sequence at the head and tail (each rod is 1 m long), the sensor was slowly fed to the predetermined position along the borehole wall, and finally, the conveyor was withdrawn.

5.2. Analysis of Monitoring Results

On–site strain measurement was carried out continuously from the working face about 80 m from the measurement point to the end of the working face pushing through the measurement point about 20 m. It lasted 45 days from the beginning to the end of the observation. Except for the occasional power failure at the working face and the mine shut down for maintenance, the field test observation was completed normally, and the quality of the data obtained was stable and reliable. In the process of advancing the working face, the variation curve of the strain monitored by each sensor with the distance of the working face from the measuring point is shown in Figure 15.
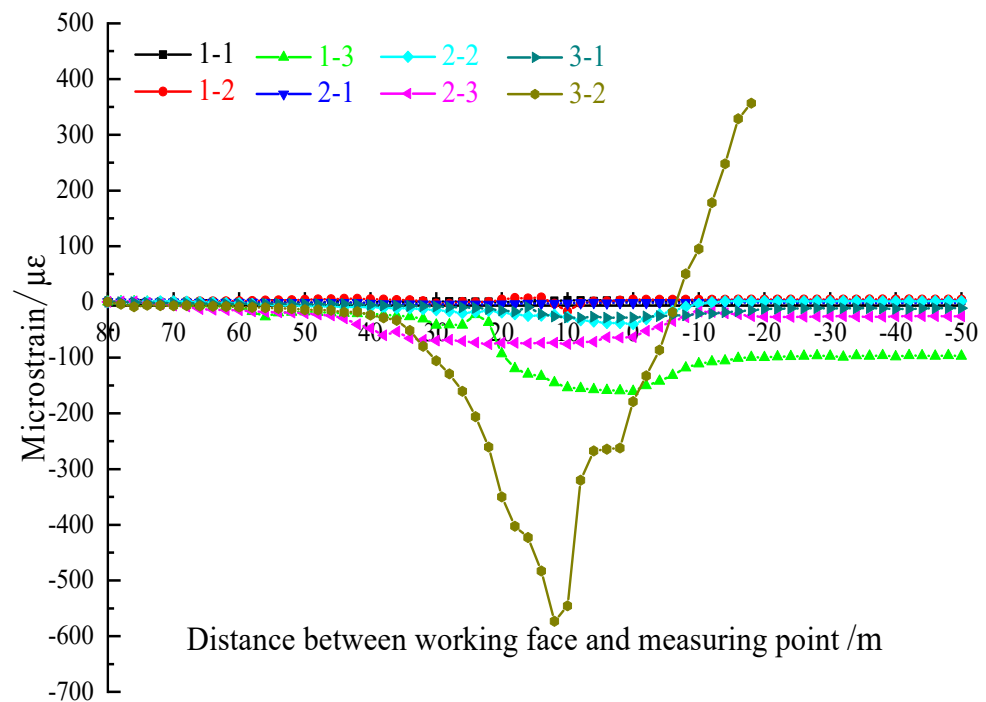
Figure 15. The strain pattern of each strain sensor during the advance of the working face.

From the analysis of Figure 15, it can be seen that:

(1)   In the vertical direction, the strain of the floor gradually decreases with the increase in the burial depth. During the advancing of the working face, the number 1–3 and 3–2 sensors undergo obvious strain changes, while the strain of the remaining sensors basically remains stable. Combined with the depth of entry and vertical depth of each sensor, it indicates that the rock damage strength shows a negative correlation trend with the burial depth of the floor.

(2)   In the horizontal direction, the strain on the floor increases gradually as the distance between the working surface and the measuring point decreases, and the strain on the floor reaches the maximum value when the working surface is within 15–25 m from the measuring point, which means that the location of the measuring point is in the peak support pressure area, and then the working surface continues to advance, and the strain on the sensor starts to rise, i.e., the peak support pressure moves forward. When the strains of sensors 1–3, 2–3, and 3–2 reached the peak, the working face was 20 m, 35 m, and 12 m away from the sensors, which means that the strains of the measurement points were affected by the mining in time and space earlier when the depth of the floor was greater, i.e., the damage often started from the deep part; in terms of the magnitude of change of the strains, they were 3–2, 1–3, and 2–3 in descending order. It indicates that the strain variation in the deep measurement points of the floor is much less than the strain in the shallow measurement points.

(3)   According to the strain curves of measurement points #1–3, the damage occurred in the range of 24 m in front of the working face, and the strain of the rock gradually increased in the early stage of damage and reached the maximum value (late stage of damage) and then smoothly transitioned and no longer changed. In addition, the curve of 2–3 measurement points at a depth of 20 m of the floor shows that the strain value reaches the maximum value at the working face 35 m from the measurement point, but the change is very small in terms of the overall change; it means that the rock at this measurement point is not obviously damaged, so the analysis shows that the damage depth of the coal seam floor is between 18.83 and 20 m.

In summary, after the slurry reinforcement of working face II633, the damage depth to the floor is between 18.83 m and 20 m. It is much smaller than the damage monitoring

depth of 29.7 m when the adjacent II632 working face is not reinforced, and the theoretical calculation result of the damage depth of the floor of the II633 working face is 26.52~31.73 m. It proves that the optimized slurry ratio greatly increases the rock strength of the floor, reduces the porosity of the floor and the damage depth affected by mining, and reduces the risk of water inrush of the floor by pre–injection reinforcement of the coal seam floor.

6. Conclusions and Discussion

6.1. Conclusions

Curtain grouting is widely used as a key technology to increase the strength and effective thickness of the floor aquiclude and reduce the risk of water inrush during safe mining on deep confined water, but due to the problems such as unclear grasp of mine hydrogeology, imperfect grouting technology or unscientific slurry proportioning, the grouting effect is poor and cannot effectively seal the fissures in the floor aquiclude, there are blind areas for grouting, or the grouting cost is high, so the expected grouting target is not achieved.

In this paper, according to the actual geological conditions of the mine, mining on deep high confined water, by using plasticity theory and empirical formula to accurately grasp the depth of damage of the floor, comparing the number of water inrush coefficient with the critical water inrush coefficient in the Huaibei mine area to accurately assess the risk of water inrush in the floor, using single cause experiment and response surface analysis method to determine the optimal ratio of grouting materials, and finally using the strain method to conduct industrial field tests to evaluate the effect of grouting. This has some guiding significance for safe, efficient, and green mining of coal seams on deep, high, confined water. The main conclusions are as follows:

(1) In coal seam mining on deep confined water, the floor is affected by the coupling effect of mining disturbance and confined water, and it can be obtained from the plastic zone theory that the plastic damage area can be divided into three areas according to the distribution of mining stress: active stress area of coal seam floor, the deformation transition area of the floor, and passive stress area of floor damage. Furthermore, the development depth of the plastic zone of the floor is related to the depth of the coal seam, mining height, cohesion, and the internal friction angle of the coal seam. The maximum depth of the floor plastic zone is 31.73 m, and the floor damage depth is 26.52 m using the empirical formula; the thickness of the key layer of the floor water barrier is between 22.14 and 27.35 m, and the water inrush coefficient T is 0.196~0.24 MPa/m. The thickness of the key layer of the floor is between 22.14 and 27.35 m, and the water inrush coefficient T is 0.196~0.24 MPa/m, which is greater than the critical water inrush coefficient Ts in the Huaibei mining area (the critical value of water inrush in the complete floor is 0.1 MPa/m, while the critical value of water inrush in the incomplete floor is 0.06 MPa/m). It is thus judged that the working face has a greater threat of water inrush during the mining process;

(2) According to the engineering practice, Na–bentonite, naphthalene series water–reducing agent, and sodium silicate were selected as the additives of grouting materials, and the slurry water separating proportion, viscosity, setting time, and the compressive strength of the grouting stone body were used as the slurry performance evaluation indexes. By designing single–factor experiments and comparing the performance indexes of slurry under single variable conditions, it was finally determined that: the range of water–cement ratio was 0.6–1; the range of bentonite dosing was 1–3%; the range of water–reducing agent dosing was 0.4–0.8%, and the optimal range of sodium silicate dosing was 1–3%.

(3) Considering the two–two interaction effects between the different influencing factors and single–factor quadratic effects, on the basis of single–factor experiments to determine the selection range of each influencing factor, a second–order response surface model was established to analyze the response of the combined scores of water separating proportion, viscosity, setting time, and compressive strength, and the CRITIC

weight method was used to objectively assign weights to each influencing factor to quantify the influence weight of each influencing factor on the slurry performance. The final weights of each factor were 0.1, 0.427, 0.304, and 0.169 for water separating proportion, viscosity, setting time, and compressive strength of the grouting stone body, respectively. A comprehensive scoring response model was established by multiple regression fitting, comparing the residual normal probability, and the residual results of the prediction model showed that the predicted and measured values were in good agreement. Through the interaction of the influencing factors, the optimal ratios of the modified slurry were determined as follows: water–cement ratio 0.8, bentonite 2%, water–reducing agent 0.6%, and sodium silicate 2%.

(4) In the industrial field test, the grouting borehole was designed with three openings, and the floor strain method was used to monitor the damage depth of the floor in real–time. Through analysis and monitoring, the law of the gradual decrease in the floor strain from shallow to deep was revealed. Comprehensive analysis shows that the damage depth of the floor is between 18.83 and 20 m, which is much smaller than the damage depth before the floor grouting reinforcement (26.52–31.73 m), indicating that the optimized slurry ratio can achieve a better grouting effect, significantly reduce the damage depth of the floor, and effectively reduce the threat of floor water inrush.

6.2. Discussion

In this paper, the failure characteristics and depth of the bottom plate and the optimal mixing ratio of slurry additives during mining on confined water are studied in depth. Combined with the field, the strain method was used to verify the failure depth of the bottom plate behind the Pearl River, and good results are achieved. However, there are still some shortcomings in the research of this paper: when testing the slurry quality indicators, only the water–cement ratio, viscosity, setting time, and compressive strength are considered, and the indexes such as the pH, temperature, adhesion, and slurry film performance are not considered and tested. In future research work, the influence of other indicators on the slurry quality and grouting effect should be emphasized.

Author Contributions: Conceptualization, W.W. and Y.Y.; methodology, W.W. and X.L.; software, Z.Q.; investigation, Y.X. and K.D.; resources, Y.Y. and X.L.; data curation, W.W. and C.Y.; writing—original draft preparation, W.W.; writing—review and editing, Y.Y., X.L. and Z.C.; project administration, W.W. and X.L.; funding acquisition, Y.Y. All authors have read and agrNovel asymmetrical bis–surfactants with naphthalene and two amide groups: Synthesis, foamability and foam stabilityeed to the published version of the manuscript. All authors have read and agreed to the published version of the manuscript.

Data Availability Statement: The data used to support the findings of this study are included within the article.

Conflicts of Interest: The authors declare no conflict of interest.

References

1. Zhu, C.; Yuan, Y.; Wang, W.; Chen, Z.; Zhong, H. Research On the "Three Shells" Cooperative Support Technology of Large-Section Chambers in Deep Mines. *Int. J. Min. Sci. Technol.* **2021**, *31*, 665–680. [CrossRef]
2. Ding, K.; Wang, L.; Wang, W.; Wang, K.; Jiang, C. Study On the Development Height of Overburden Water-Flowing Fracture Zone of the Working Face. *Geofluids* **2021**, *2021*, 1–10. [CrossRef]
3. Yuan, Y.; Yuan, C.; Zhu, C.; Liu, H.; Wang, S. Study On the Disaster Reduction Mechanism of Presplitting Blasting and Reasonable Blasting Parameters for Shallowly Buried Remnant Pillars. *Energy Sci. Eng.* **2019**, *7*, 2884–2894. [CrossRef]
4. Yuan, Y.; Chen, Z.; Yuan, C.; Zhu, C.; Zhang, X. Numerical Simulation Analysis of the Permeability Enhancement and Pressure Relief of Auger Mining. *Nat. Resour. Res.* **2019**, *29*, 931–948. [CrossRef]
5. Zhu, C.; Yuan, Y.; Chen, Z.; Meng, C.; Wang, S. Study of the Stability Control of Rock Surrounding Longwall Recovery Roadways in Shallow Seams. *Shock Vib.* **2020**, *2020*, 1–22. [CrossRef]

6. Ma, K.; Yin, L.M.; Chen, J.T.; Chen, M.; Cui, B.Q. Theoretical Analysis On Failure of Water-Resisting Key Strata in the Floor by Local High Confined Water in Deep Mining. *Rock Soil Mech.* **2018**, *39*, 3213–3223.

7. Hu, Y.; Li, W.; Wang, Q.; Liu, S.; Wang, Z. Evolution of Floor Water Inrush From a Structural Fractured Zone with Confined Water. *Mine Water Environ.* **2019**, *38*, 252–260. [CrossRef]

8. Zhang, T.; Zhao, Y.; Gan, Q.; Nie, X.; Zhu, G.; Hu, Y. Investigations Into Mining-Induced Stress-Fracture-Seepage Field Coupling in a Complex Hydrogeology Environment: A Case Study in the Bulianta Colliery. *Mine Water Environ.* **2019**, *38*, 632–642. [CrossRef]

9. Liang, Z.; Song, W.; Liu, W. Theoretical Models for Simulating the Failure Range and Stability of Inclined Floor Strata Induced by Mining and Hydraulic Pressure. *Int. J. Rock Mech. Min.* **2020**, *132*, 104382. [CrossRef]

10. Zhu, C.; Yuan, Y.; Yuan, C.; Liu, F.; Chen, Z.; Wang, S. Study On the Structural Forms of the Key Strata in the Overburden of a Stope During Periodic Weighting and the Reasonable Working Resistance of the Support. *Energy Sci. Eng.* **2020**, *8*, 2599–2620. [CrossRef]

11. Yang, B.; Yuan, J.; Ye, Z. Risk Assessment of Coal Mining Above Confined Aquifer Based On Maximizing Deviation in a Gis Environment. *Arab. J. Geoences* **2018**, *11*, 299. [CrossRef]

12. Lu, Y.; Wang, L. Numerical Simulation of Mining-Induced Fracture Evolution and Water Flow in Coal Seam Floor Above a Confined Aquifer. *Comput. Geotech.* **2015**, *67*, 157–171. [CrossRef]

13. Yu, S.; Xu, J.; Zhu, W.; Wang, S.; Liu, W. Development of a Combined Mining Technique to Protect the Underground Workspace Above Confined Aquifer From Water Inrush Disaster. *Bull. Eng. Geol. Environ.* **2020**, *79*, 3649–3666. [CrossRef]

14. Lu, Z.; Ju, W.; Yin, X.; Sun, Z.; Han, C. Mechanical Analysis of the Failure Characteristics of Stope Floor Induced by Mining and Confined Aquifer. *Shock Vib.* **2021**, *2021*, 1–13. [CrossRef]

15. Sun, J.; Miao, X. Water-Isolating Capacity of an Inclined Coal Seam Floor Based On the Theory of Water-Resistant Key Strata. *Mine Water Environ.* **2017**, *36*, 310–322. [CrossRef]

16. Yu, X.G.; Han, J.; Shi, L.Q.; Wei, J.C.; Li, S.C. Forecast of Destroyed Floor Depth Based On Bp Neural Networks. *J. China Coal Soc.* **2009**, *34*, 731–736.

17. Wang, W.; Yuan, Y.; Chen, Z.; Zhu, C. Physical Modeling of Floor Failure Above Confined Water: A Case Study in China. *Environ. Earth Sci.* **2022**, *81*, 352. [CrossRef]

18. Xu, Y.C.; Yang, Y. Applicability Analysis On Statistical Formula for Failure Depth of Coal Seam Floor in Deep Mine. *Coal Sci. Technol.* **2013**, *41*, 129–132.

19. Ma, K.; Sun, X.Y.; Tang, C.A.; Yuan, F.Z.; Wang, S.J.; Chen, T. Floor Water Inrush Analysis Based On Mechanical Failure Characters and Microseismic Monitoring. *Tunn. Undergr. Space Tech.* **2020**, *108*, 103698. [CrossRef]

20. Song, W.; Liang, Z. Theoretical and Numerical Investigations On Mining-Induced Fault Activation and Groundwater Outburst of Coal Seam Floor. *Bull. Eng. Geol. Environ.* **2021**, *80*, 5757–5768. [CrossRef]

21. Liang, Z.; Song, W. Theoretical and Numerical Investigations of the Failure Characteristics of a Faulted Coal Mine Floor Above a Confined Aquifer. *Mine Water Environ.* **2021**, *40*, 456–465. [CrossRef]

22. Yang, C.; Zhu, S.; Wang, Z.; Li, F. Deformation and Failure of Floor in Mine with Soft Coal, Soft Floor, Hard Roof and Varying Thicknesses of Coal Seam. *Eng. Fail. Anal.* **2020**, *115*, 104653.

23. Li, A.; Mu, Q.; Ma, L.; Liu, C.; Wang, S.; Wang, F.; Mou, L. Numerical Analysis of the Water-Blocking Performance of a Floor with a Composite Structure Under Fluid–Solid Coupling. *Mine Water Environ.* **2021**, *40*, 479–496. [CrossRef]

24. Zhu, S.; Jiang, Z.; Cao, D.; Qiang, S.; Yang, C. Restriction Function of Lithology and its Composite Structure to Deformation and Failure of Mining Coal Seam Floor. *Nat. Hazards* **2013**, *68*, 483–495.

25. Zhou, W.; Zhang, P.; Wu, R.; Hu, X. Dynamic Monitoring Study On the Characteristics of Deformation and Failure of Extra-Thick Coal Seam Floor in Deep Mining. *J. Appl. Geophys.* **2019**, *163*, 132–138. [CrossRef]

26. Yu, X.; Liu, Y.; Fan, H. Influence of Coal Seam Floor Damage On Floor Damage Depth. *Environ. Earth Sci.* **2022**, *81*, 192. [CrossRef]

27. Chang, J.; Li, D.; He, K. Mining Failure Response Characteristics of Stope Floor: A Case of Renlou Coal Mine. *Adv. Civ. Eng.* **2020**, *2020*, 1–11. [CrossRef]

28. Zhou, J.R.; Yang, T.H.; Zhang, P.H.; Xu, T.; Wei, J. Formation Process and Mechanism of Seepage Channels Around Grout Curtain From Microseismic Monitoring: A Case Study of Zhangmatun Iron Mine, China. *Eng. Geol.* **2017**, *226*, 301–315. [CrossRef]

29. Zhou, F.; Sun, W.; Shao, J.; Kong, L.; Geng, X. Experimental Study On Nano Silica Modified Cement Base Grouting Reinforcement Materials. *Geomech. Eng.* **2020**, *1*, 67–73.

30. Liu, S.; Fei, Y.; Xu, Y.; Huang, L.; Guo, W. Full-Floor Grouting Reinforcement for Working Faces with Large Mining Heights and High Water Pressure: A Case Study in China. *Mine Water Environ.* **2020**, *39*, 268–279. [CrossRef]

31. Zhang, S.; Guo, W.; Li, Y.; Sun, W.; Yin, D. Experimental Simulation of Fault Water Inrush Channel Evolution in a Coal Mine Floor. *Mine Water Environ.* **2017**, *36*, 443–451. [CrossRef]

32. Xu, Z.; Sun, Y.; Gao, S.; Chen, H.; Li, X. Comprehensive Exploration, Safety Evaluation and Grouting of Karst Collapse Columns in the Yangjian Coalmine of the Shanxi Province, China. *Carbonates Evaporites* **2021**, *36*, 16. [CrossRef]

33. Cao, S.G.; Yao, Q.L.; Wang, F.H.; Jiang, H.J. Analysis of Water Inrush Risk From Coal Seam Floor Over a Confined Water Body. *J. Min. Saf. Eng.* **2010**, *27*, 346–350.

34. Hu, Y.; Li, W.; Wang, Q.; Liu, S.; Wang, Z. Study On Failure Depth of Coal Seam Floor in Deep Mining. *Environ. Earth Sci.* **2019**, *78*, 697. [CrossRef]

35. Wei, Z.; Zhang, D.; Qi, D.; Hu, W.; He, Z.; Zhang, W. Floor Failure Depth of Upper Coal Seam During Close Coal Seams Mining and its Novel Detection Method. *Energ Explor. Exploit.* **2018**, *36*, 1265–1278.

36. Jiang, Y.; Cai, T.; Zhang, X. A Multifactor Coupling Prediction Model for the Failure Depth of Floor Rocks in Fully Mechanized Caving Mining: A Numerical and in Situ Study. *R. Soc. Open Sci.* **2019**, *6*, 190528. [CrossRef] [PubMed]

37. Liu, W.; Mu, D.; Xie, X.; Li, Y.; Wang, D. Sensitivity Analysis of the Main Factors Controlling Floor Failure Depth and a Risk Evaluation of Floor Water Inrush for an Inclined Coal Seam. *Mine Water Environ.* **2017**, *37*, 636–648. [CrossRef]

38. Xu, Y.C. Design Methods of the Effective Water-Resisting Thickness for the Protective Seam of the Water Barrier in Fully-Caving Mechanized Coal Mining. *J. China Coal Soc.* **2005**, *30*, 305–308.

39. Shi, L.; Qiu, M.; Wang, Y.; Qu, X.; Liu, T. Evaluation of Water Inrush From Underlying Aquifers by Using a Modified Water-Inrush Coefficient Model and Water-Inrush Index Model: A Case Study in Feicheng Coalfield, China. *Hydrogeol. J.* **2019**, *27*, 2105–2119. [CrossRef]

40. Liu, U. Ft-ir and xrd analysis of natural na-bentonite and cu(ii)-loaded na-bentonite. *Spectrochim. Acta Part A: Mol. Biomol. Spectrosc.* **2011**, *79*, 1013.

41. Yue, J.A.; Xg, B.; Lj, A.; Zz, A.; Rui, Y.A.; Yu, Z.A.; Sun, H. Novel asymmetrical bis-surfactants with naphthalene and two amide groups: Synthesis, foamability and foam stability. *J. Mol. Liq.* **2021**, *329*, 115534.

42. Song, J.H.; Kang, J.Y.; Koo, J.S. Proposal of modified (normalized) astm offset method for determination of fatigue crack opening load. *Int. J. Fatigue* **2005**, *27*, 293–303. [CrossRef]

43. Li, W.; Liu, Y.; Qiao, W.; Zhao, C.; Yang, D.; Guo, Q. An Improved Vulnerability Assessment Model for Floor Water Bursting From a Confined Aquifer Based On the Water Inrush Coefficient Method. *Mine Water Environ.* **2018**, *37*, 196–204. [CrossRef]

44. Sun, Y.; Zhang, P.; Yan, W.; Wu, J.; Yan, F. Grouting Material Development and Dynamic Grouting Test of Broken Rock Mass. *J. Mater. Civ. Eng.* **2022**, *34*, 4022072. [CrossRef]

45. Gang, Z.A.; Jh, A.; Yu, D.A.; Ma, A.; Su, Y.; Jiao, C.; Chen, H. Experimental Study On Preparation and Optimization of High-Performance Cement Grouts Mixed with Chemical Additives for Capsule Grouting Technology—Sciencedirect. *J. Mater. Res. Technol.* **2022**, *17*, 1469–1484.